Journal of Environmental Management 230 (2019) 266–281

Contents lists available at ScienceDirect

Journal of Environmental Management

journal homepage: www.elsevier.com/locate/jenvman

Research article

# Utilizing of neodymium vanadate nanoparticles as an efficient catalyst to boost the photocatalytic water purification

Rozita Monsef, Maryam Ghiyasiyan-Arani, Masoud Salavati-Niasari*

*Institute of Nano Science and Nano Technology, University of Kashan, Kashan, P. O. Box. 87317-51167, I. R., Iran*

ARTICLE INFO

*Keywords:*
$NdVO_4$
Nanostructures
Eriochorome Black T
Photocatalytic degradation
Nano-catalyst
Recyclability

ABSTRACT

Neodymium Vanadate ($NdVO_4$) nanostructures were successfully synthesized *via* a modified solid state method in the presence of ligand. These nanoparticles were further used as a photocatalyst. Primarily the best structural formations and smallest crystallite sizes of the systems were identified and optimized by changing the calcination time, calcination temperature and molar ratio of the ligand. The cationic (Methyl Violet (MV)), and anionic (Eosin Y (EY) and Eriochrome Black T (EBT)) dyes were used as a model to evaluate the photoactivity under UV–Vis irradiation. Several operational factors were examined to improve the photocatalytic efficiency include type of dye, type of light source, pH and dye concentration. As a result, the best efficiency in 5 ppm Eriochorome Black T at pH = 11 was achieved in the presence of 0.05 g $NdVO_4$ nanocatalysts.

## 1. Introduction

The organic dyes (cationic and anionic dyes) are one of the most important environmental pollutants that are used in various industries such as textile, paper printing and pulp, rubber, plastics, leather, cosmetics, etc (Şahin et al., 2013; Elijah and Nwabanne, 2014). Aquatic environmental deterioration is a serious issue due to rapid urbanization and economic development; hence, the reductions of the hazardous contaminants from waste water are urgently required. Electroactive nanocatalysts are recently achieved a great attention in order to remove colorants from aquatic environments. $M_x$ - orthovanadates (M: Na, Ca, Ba, Sc, Er, Nd …) are the inorganic compounds which consider for this application (Mahapatra et al., 2007). Among these compounds, neodymium vanadate is an important category of rare earth (RE) orthovanadates that has been synthesized by various techniques such as hydrothermal (Wu et al., 2005), solid-state reaction (Errandonea et al., 2014), sonochemical (Monsef et al., 2018), precipitation (Vosoughifar, 2016), sol-gel (Au et al., 1996) and microwave (Mahapatra et al., 2008a). $NdVO_4$ powders are renowned as promising materials in photocatalytic, electrical, catalytic, laser, photoluminescence, optic, phosphors, polarizer properties (Mahapatra et al., 2008b; Yuvaraj et al., 2014; Selvan et al., 2009; Yao et al., 2010; Verma et al., 2016; Deng et al., 2008; Nguyen et al., 1997). Rare earth orthovanadates, especially in nanosized state, are highly promising for biomedical applications due to their high stability and nontoxicity (Lyadov and Kurilkin, 2016). Moreover, transition metal vanadates have been also reported for various academic and industrial applications; for example cobalt vanadate, copper vanadate, nickel vanadate, iron and zinc vanadate (Ghiyasiyan-Arani et al., 2016a, 2016b, 2016c, 2017, 2018; Ghiyasiyan-Arani and Masjedi-Arani, 2016; Mazloom et al., 2016).

In recent years, nanoscale neodymium vanadate has been achieved a great interest in its effective photocatalytic properties. It has been found that $NdVO_4$ as a wide-bandgap semiconductor with a zircon-type structure and I41/ amd space group shows a photocatalytic activity for degradation of organic contaminants which is comparable or even higher than that of the commercial $TiO_2$ (Dragomir et al., 2013). But due to its wide band gap (> 3 eV), NdVO4 is a UV active material. However, the previous research indicates under visible light, approximately 66% of RhB can be degraded by the catalysis of $NdVO_4$ nanowires over 6 h of illumination. This degradation can be attributed to the electron transitions of 4f electrons, the regular $VO_4$ tetrahedra. The regular $VO_4$ tetrahedra and $Nd^{3+}$ of $NdVO_4$ play a crucial role in the photocatalytic process (Jing et al., 2011). In the current study, neodymium vanadium oxide was synthesized *via* a traditional solid state method in the presence of $H_2$acacen ligand as a Schiff base capping agent. This method is known as a facile, low-cost, green and solvent-free. In the literatures, the $NdVO_4$ powders have been prepared by SSR (Solid state reaction) method, where the particles are in the range of 1–5 μm (Dragomir et al., 2013); however, in this work, nanoscaled $NdVO_4$ ceramics are formed (~80 nm) and optimized by changing experimental conditions. These nanoceramics play a potential role as an impressive semiconductor in photocatalysis process for degradation of

* Corresponding author.
*E-mail address:* salavati@kashanu.ac.ir (M. Salavati-Niasari).

https://doi.org/10.1016/j.jenvman.2018.09.080
Received 21 May 2018; Received in revised form 18 September 2018; Accepted 22 September 2018

**Table 1**
Preparation conditions of $NdVO_4$ by solid state method.

| Sample No. | Solvent | Schiff-base ligand | Molar ratio (Nd:$H_2$acacen) | Calcination temperature (°C) | Time(h) | Product |
|---|---|---|---|---|---|---|
| 1 | – | – | – | 700 | 6 | $NdVO_4$ |
| 2 | – | $H_2$acacen | 1:0.5 | 700 | 6 | $NdVO_4$ |
| 3 | Methanol | $H_2$acacen | 1:0.5 | 700 | 6 | $NdVO_4$ |
| 4 | Methanol | $H_2$acacen | 1:1 | 700 | 6 | $NdVO_4$ |
| 5 | Methanol | $H_2$acacen | 1:2 | 700 | 6 | $NdVO_4$ |
| 6 | Methanol | $H_2$acacen | 1:2 | 700 | 4 | $NdVO_4$ |
| 7 | Methanol | $H_2$acacen | 1:2 | 700 | 2 | $NdVO_4$ |
| 8 | Methanol | $H_2$acacen | 1:2 | 600 | 2 | $NdVO_4/Nd_2O_3$ |
| 9 | Methanol | $H_2$acacen | 1:2 | 500 | 2 | $NdVO_4/Nd_2O_3/V_2O_5$ |

organic dyes. Eriochrome Black T, Methyl Violet, and Eosin Y were selected as pollutants; Eriochrome Black T is an azo dye that is used for intinction silk and wool (Vaiano et al., 2017), Eosin Y and Methyl Violet are anionic and cationic dyes used in ink and textile industries (Oyelude et al., 2017; Mendhulkar Vijay et al.,).

Our study aims to provide optimal frameworks in the synthesis of pure, uniform and nanoscale catalysts by applying Schiff-base ligand and also changing the synthesis conditions. Stability and recyclability of $NdVO_4$ nanoparticles is an important factor in water treatment. Effect of different parameters on photoactivity of the samples such as effect of type of dye, type of irradiation source, pH and dye concentration was investigated to improve efficiency of catalyst function.

## 2. Experimental

### 2.1. Materials and method

All reagents for the preparation of $NdVO_4$ nanoparticles such as neodymium nitrate hexahydrate ($Nd(NO_3)_3.6H_2O$), ammonium metavanadate ($NH_4VO_3$), methanol, ethylenediamine (en) were purchased from Merck Company and used as received without further purification. Bis (acetyl acetanato) ethylene diamine Schiff base ($H_2$acacen) was prepared to consider the published procedure (Motahari et al., 2015). Briefly, the stoichiometric amounts of acetylacetonate solution and ethylenediamine were heated in 40 ml ethanol under reflux for 4 h. The product was separated and washed with ethanol and dried overnight in an oven at 60 °C.

$NdVO_4$ nanostructures were synthesized by a general solid state reaction in the air using $Nd(NO_3)_3{\cdot}6H_2O$ and $NH_4VO_3$ as the starting materials in the presence of the as-prepared $H_2$acacen Schiff-base. In a typical experiment, 0.25 g of $Nd(NO_3)_3.6H_2O$ and 0.067 g $NH_4VO_3$ (Nd:V/1:1) were grinded carefully, and then various amounts of $H_2$acacen were added. The admixture was further milled by zirconia ball-mill for 30 min using 5 drops methanol as a solvent and homogenizing agent. The reaction admixture was dried and calcined in an alumina crucible at 500, 600 and 700 °C. The preparation conditions are summarized in Table 1.

### 2.2. Characterizations

The phase structure of the products was identified using X-ray powder diffraction measurements) Philips-X'pertpro (by Ni filter and Cu Ka lines as a radiation source (λ = 1.54 Å). Fourier transform infrared (FT-IR) spectra of the samples diffused in KBr pellets were obtained using Nicolet Magna- 550 spectrometer at room temperature. The morphology and particle sizes of the samples were observed using a LEO-1455VP scanning electron microscope (SEM) and transmission electron microscope (TEM) by a Philips EM208 operating at an accelerating voltage of 200 kV. The energy dispersive spectrometry (EDS) was used in order to determine the elements of compounds with an accelerating voltage of 20 kV. Solid UV–Visible diffuse reflectance spectrometer (DRS) was performed with a Shimadzu UV-3101PC, UV/Vis spectrophotometer. The magnetic properties of the $NdVO_4$ were studied by a vibrating sample magnetometer (VSM, Meghnatis Kavir Kashan Co., Kashan, Iran).

### 2.3. Photocatalytic measurement

To inquire the photocatalytic activity of the $NdVO_4$ nanoparticles, a series of control experiments was carried out. Photodecolorization experiments were conducted in a photoreactor using a 400 W mercury lamp and 400 W Osram lamps as the irradiation sources at room temperature. Experimentally, an exact amount of the $NdVO_4$ sample (0.05 g) was added in to the organic pollutant solutions (Eriochrome Black T, Methyl Violet, Eosin Y) in different conditions. The above suspension was transferred into the reactor, stirred and aerated in the dark for 30 min to attain adsorption-desorption equilibrium between the catalyst and dye substrates. This suspension was subjected to light irradiation where 5 ml of the solution was taken at certain times. At the end of the experiment, the samples were centrifuged to separate the catalysts. Concentration and absorbance of dye solutions was determined by UV–vis spectrophotometer. The amount of dye degradation (D.P.) with standard deviation at the sampling time was calculated by means of Eq. (1). In this equation, $C_0$ and $C_t$ are the absorbance quantity of the sample at 0 and t minute, respectively (Error bars in the Fig. 11 are standard deviations in average percentage destruction).

$$D.P.(t) = \frac{C_0 - C_t}{C_0} \times 100 \quad (1)$$

## 3. Result and discussion

### 3.1. Phase compositions and morphological observations

#### 3.1.1. X-ray diffraction patterns

The XRD patterns were used to identify the phase structures of $NdVO_4$ powders (Fig. 1(a-c)). The results indicate that all the samples are highly pure and crystalline. The diffraction peaks can be ascribed to the tetragonal phase of $NdVO_4$ (JCPDS 15-0769; space group: 141/amd). In order to study the effect of temperature and time on the lattice structure of $NdVO_4$, the respective diffractograms (Fig. 2(a-d)) indicate that the samples (Samples 8 and 9) at reduced calcination temperatures

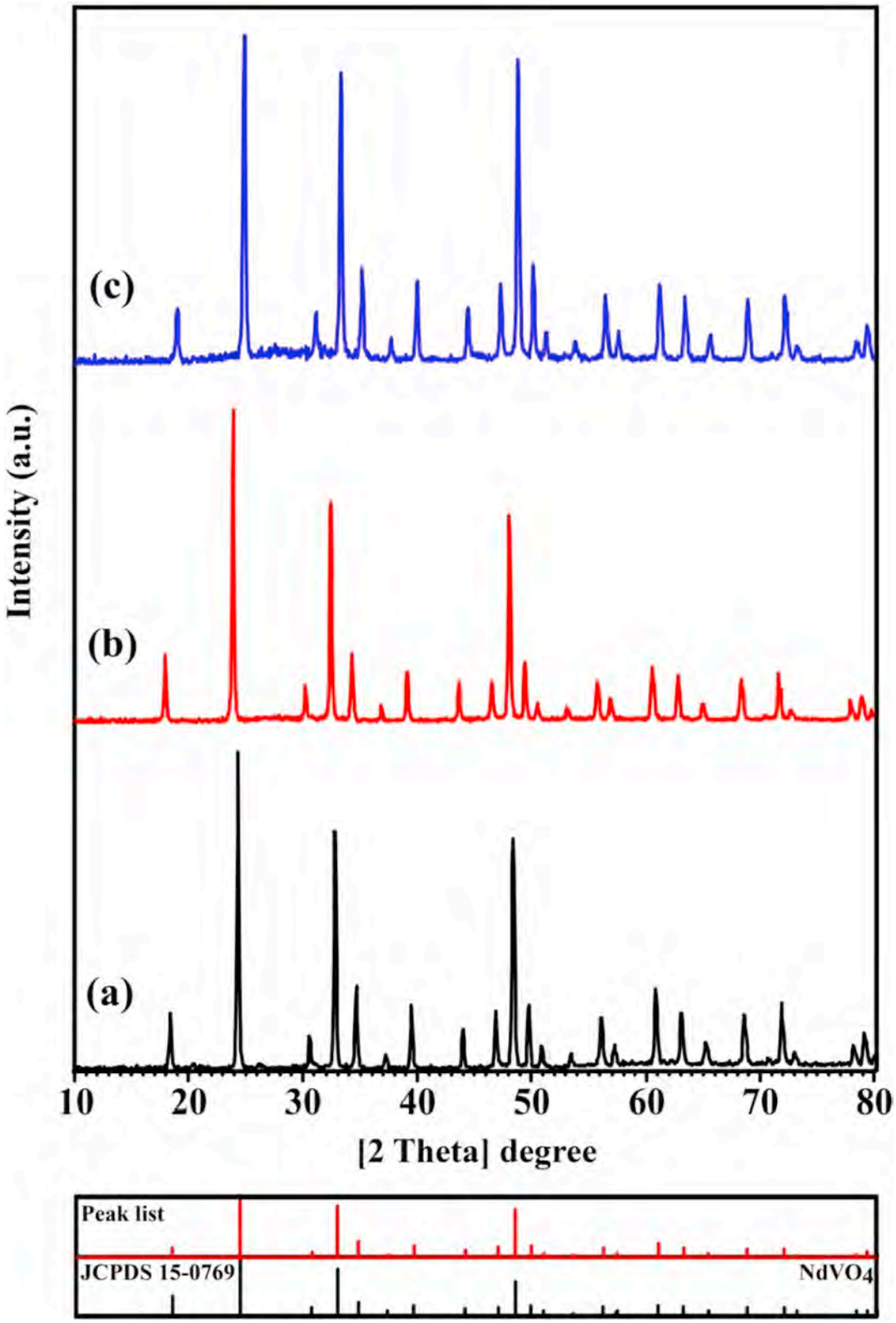


**Fig. 1.** XRD patterns of $NdVO_4$ synthesized at 700 °C with different molar ratios of Nd: $H_2$acacen (a) 1:0.5 (sample No.3), (b) 1:1 (sample No.4) and (c) 1:2 (sample No.5).

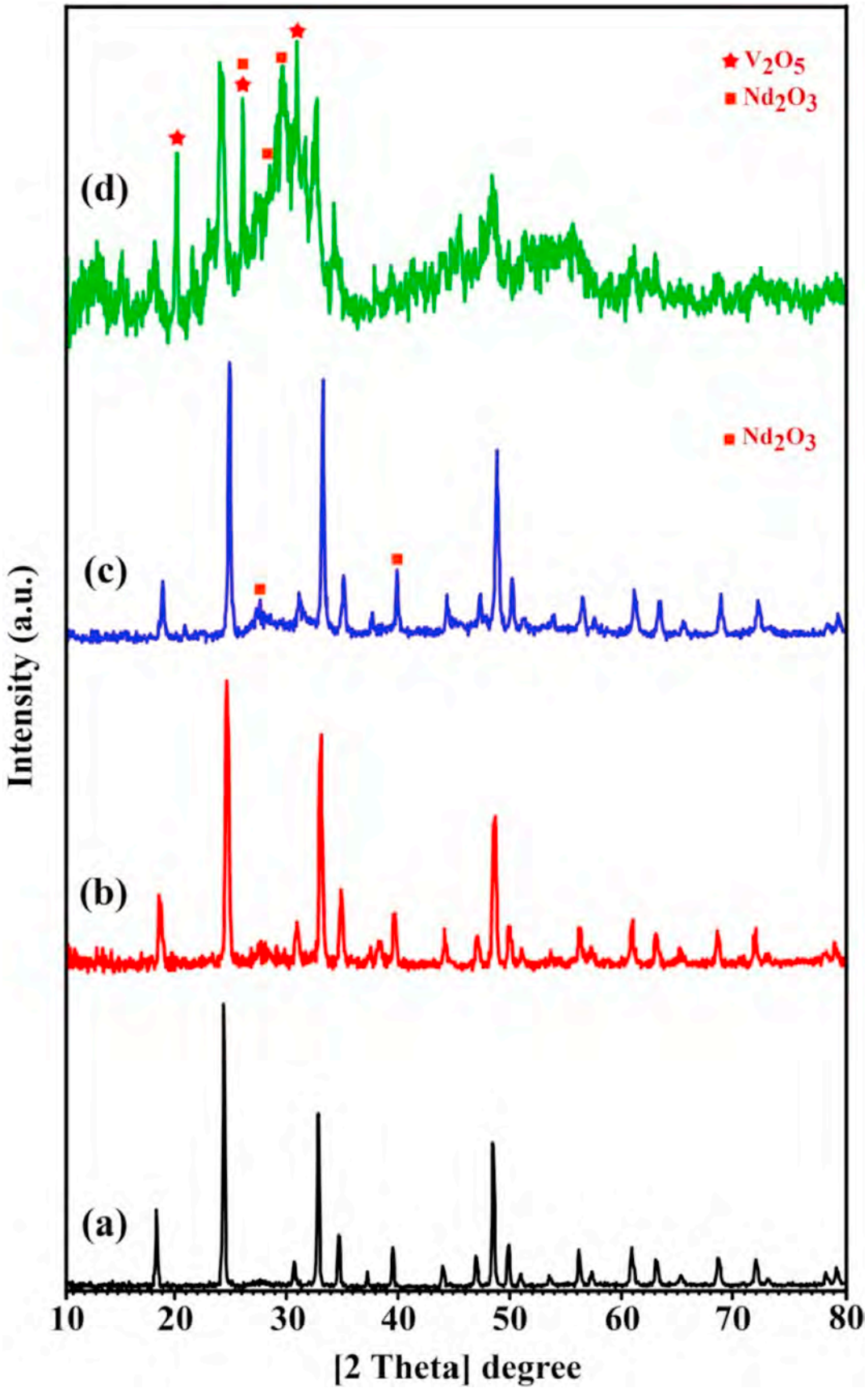


**Fig. 2.** XRD patterns of the products synthesized by molar ratio of Nd: $H_2$acacen (1:2) at different calcination temperatures and different calcination times (a) sample No.6, (b) sample No.7 and (c) sample No.8 and (d) sample No.9.

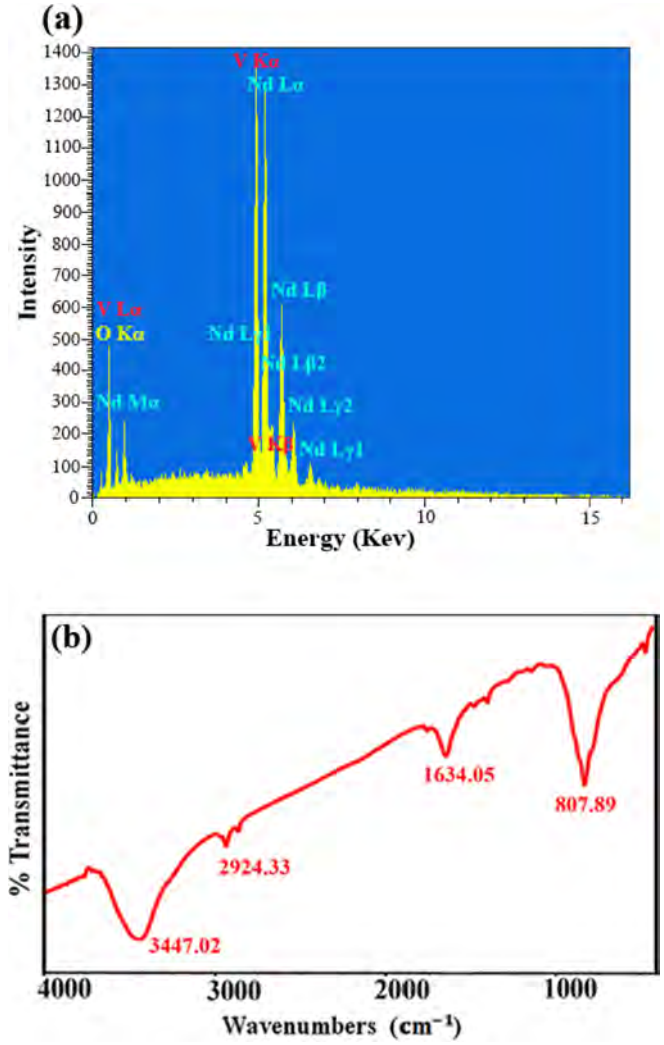


**Fig. 3.** (a) EDS pattern and (b) FT-IR spectra of $NdVO_4$ nanostructure (sample No. 7).

are well-matched with $NdVO_4$ (JCPDS 15-0769); however, minor impurities can be observed. The XRD pattern of the sample No. 8 (Fig. 2c) shows two diffraction peaks at $2\theta = 27.31^{\circ}$ and $39.66^{\circ}$, which is indexed to the hexagonal $Nd_2O_3$ (JCPDS 83-1353). The extent of impurities in the sample 9 (Fig. 2d) are much higher containing a mixture of $NdVO_4$, $Nd_2O_3$ and $V_2O_5$. The peaks grow at $2\theta = 20.37^{\circ}$, $26.31^{\circ}$ and $30.15^{\circ}$ are matched with the orthorhombic phase of $V_2O_5$ (JCPDS 01-0359). These results suggest that the calcination temperatures play an important role in controlling the purity of the products and increasing temperature from 500 °C to 700 °C promote crystallization of the products, while changing the calcination time (Fig. 2a and b) have no effect on lattice structures. From the results, it is obvious that the sample 9 shows lower crystallinity and phase purity as compared to the other samples. From the XRD data, the average crystallite sizes of the samples are calculated using Scherer equation (Klung and Alexander, 1962) and tabulated in Table 2.

### 3.1.2. EDX and FT-IR analysis

The elemental analysis of the sample, $NdVO_4$ nanostructures (Fig. 3a), confirms the coexistence of Neodymium, Vanadium and Oxygen elements. Energy dispersive X-ray analysis indicated uniform distributions for all elements involved. The bond formations of the $NdVO_4$ were studied by recording its respective FTIR spectrum in the region of 400–4000 $cm^{-1}$ (Fig. 3b). A vibration frequency at 807 $cm^{-1}$ is originated from V—O bond. The peak related to C—H (2924 $cm^{-1}$) appears in the spectrum confirms that the $CH_2$ and $CH_3$ groups of hydrocarbon moiety are still present due to the nanoparticles and ligand reaction profiles. The absorption bands around 1634 $cm^{-1}$ and 3447 $cm^{-1}$ are due to bending and stretching vibrations of —OH groups attached to the nanoparticles surface.

### 3.1.3. SEM and TEM images

The morphology and the particle diameter of $NdVO_4$ structures were observed in its respective FESEM micrographs (Fig. 4). The shape, size, and uniformity of the samples after thermal treatment were found to be strongly depending on a reaction conditions such as calcination temperatures and molar ratio of the precursors. The surface morphology of the blank sample (without ligand and solvent) is shown in Fig. 4a. Here the micro-sized particles with approximately dense texture are formed. In the presence of the ligand (without solvent), Fig. 4b, the $NdVO_4$ particles, are still over-size, however, very small particles can be observed on the particles. Interestingly, upon increasing ethanol (dispersion agent) into the reaction container, more homogeneous nanosized particles are formed (Fig. 4 c–e) due to the effective collisions between the particles and balls during the ball-mill process. The nanosized particles (> 100 nm) with approximately homogeneous texture generate in the sample with Nd:H2acacen/1:2 (Fig. 4e); while in the samples with 1:0.5 and 1:1 molar ratios Fig. 4(c, d), massive bulk with octagon shapes exist in an obvious form. $H_2$acacen Schiff-base ligand as capping agent could adsorb on crystal facets of $NdVO_4$ and inhibits the crystal growth and thus leads to $NdVO_4$ structure consisting of nanoparticles. Upon increasing the amount of $H_2$acacen ligand up to 2 times, due to the effect of steric hindrance, a decrease in particle sizes occurs in order to obtain the best size and uniform morphology, while in lower concentrations of ligand (0.5:1 and 1:1), the particle sizes are larger. These phenomena occur due to the incomplete capping of ligand to the crystal facets, therefore, the particles grow in order to form large size structures (Scheme 1). Furthermore, calcination time for $NdVO_4$ was optimized based on the above optimum ratio. As calcination time extended from 2 h to 6 h, the $NdVO_4$ particle sizes were converted and various diameters could be obtained by controlling the time. Fig. 5 shows the FESEM images for 2, 4 and 6 h calcination times. Longer calcination may permit particles to grow into the large diameters; however, this trend is not linear. After 2 and 6 h of calcination, the smallest size of the particles obtained, while after 4 h, the size of the particles increased gradually into about 300 nm. Based on comprehensive control of preparation status, the most efficient parameters for synthesis of the $NdVO_4$ were acquired. Accordingly, sample No. 7 was selected as a most efficient sample due to the size and uniformity for photocatalytic application. To confirm the surface morphology of the best sample (No.7), the TEM images were captured (Fig. 6). Here, the TEM images contain nanoparticles, displaying small dimensions where precipitated in aggregates.

## 3.2. Magnetic and optical absorption properties

The magnetization hysteresis of $NdVO_4$ (sample No. 7) are characterized at room temperature (25 °C) though the vibrating sample magnetometer (VSM) analyzer are demonstrated in Fig. 7. The

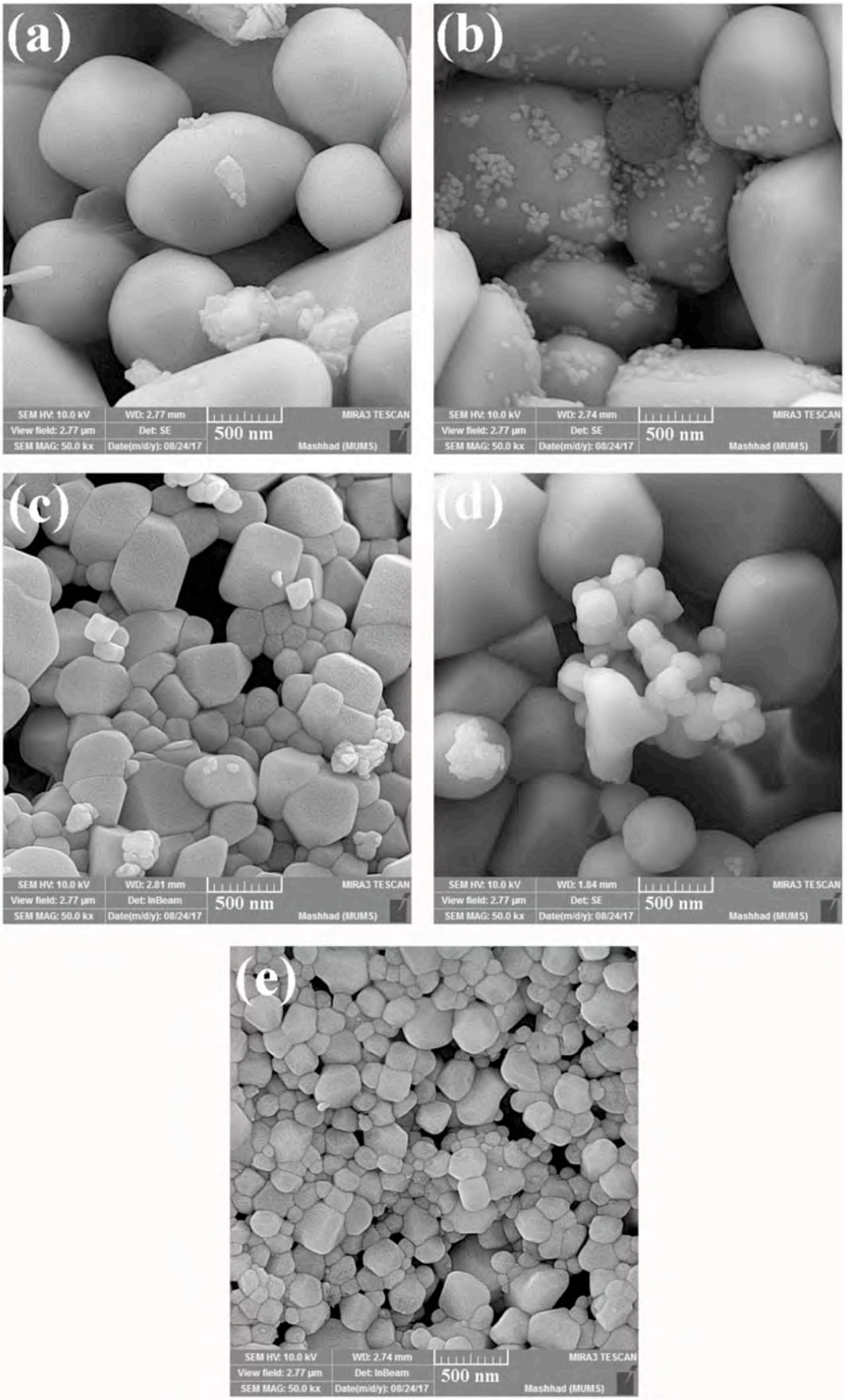


**Fig. 4.** SEM image of $NdVO_4$ samples with different molar ratios of Nd: $H_2$acacen sample No (a) 1, (b) 2, (c) 3) d) 4 and (e) 5.

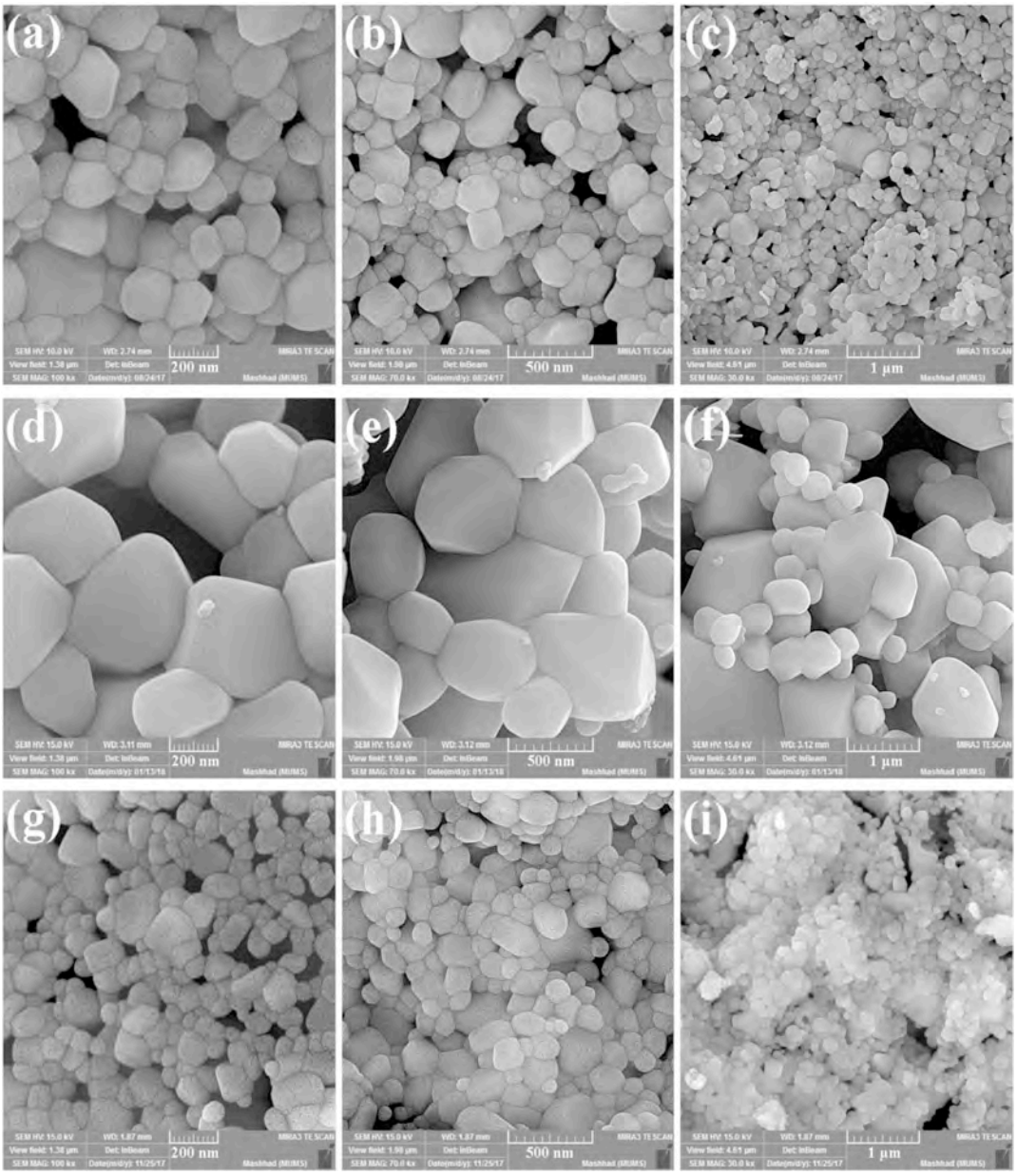


**Fig. 5.** SEM image of $NdVO_4$ samples with molar ratio of Nd: $H_2$acacen (1:2) in the presence of solvent synthesized at 700 °C and different calcination times (a–c) sample No.5, (d–f) sample No.6, (g–i) sample No.7.

hysteresis loop of the sample displays paramagnetic behavior and the maximum saturation magnetization of the sample in the most efficient condition is 0.13 emu/g.

The UV–Vis diffuse reflectance spectrum (DRS) of the sample No. 7 (Fig. 8) was used in order to measure the band gap energy. The band gap energy can be calculated from the intercept of the tangents to the plots of $(\alpha h\nu)^{1/2}$ *vs.* photon energy. The estimated band gap value is around 3.3 eV for the sample prepared in the best conditions (sample No. 7). The band gap can be used as a necessity for detection of the proper sort of illumination required for the destruction of dye.

### 3.3. Catalyst photoactivity

#### 3.3.1. Effect of dye

Fig. 9a shows the degradation of Methyl Violet (MV), Eosin Y (EY) and Eriochrome Black T (EBT) in UV light when $NdVO_4$ nanophotocatalysts were added into dye solutions. $NdVO_4$ nanoparticles can induce 30.15%,32.59% and 72.98% of decolerations at 75 min for MV, EY and EBT, respectively.

#### 3.3.2. Effect of dye concentration

Subsequently, we investigated the photocatalytic performance of the $NdVO_4$ nanoparticles with different concentration of dye solutions.

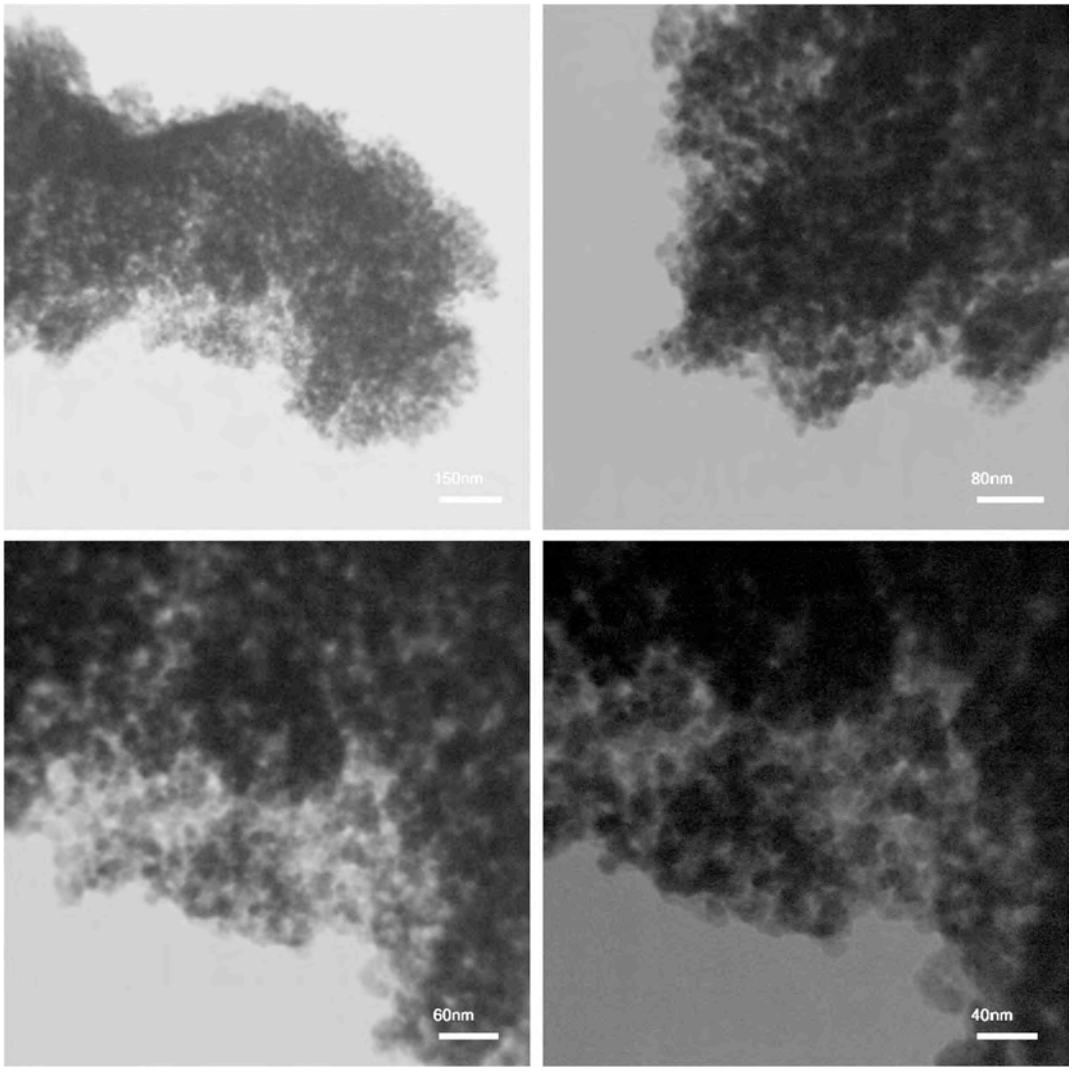


**Fig. 6.** TEM image of $NdVO_4$ in different magnification (Sample No. 7).

Fig. 9b indicates the photocatalytic efficiencies of the $NdVO_4$ nanoparticles in 5 ppm, 10 ppm and 15 ppm of EBT under UV light to be around 72.98%, 61.11% and 48.20%, respectively. In 15 ppm of EBT concentration, a greater number of EBT molecules would be saturated the binding sites found on the surface of $NdVO_4$ nanoparticles. It is obvious that the percentage of removal efficiencies decreased as the initial dye concentrations increased (de Luna et al., 2013).

### 3.3.3. Effect of pH

On the other hand, the effect of pH of the EBT solutions on the photocatalytic efficiencies was examined (Fig. 10a). The degradation efficiencies of EBT in the pH equal to 3, 7 and 11 obtain to be around 59.35%, 42.34% and 72.98%, respectively. The relationship between the initial solution pH and adsorption capacity uptake can play an important role in photocatalytic process. According to Fig. 10a, it was clear that maximum efficiency for remove dye EBT takes place at pH 3 and 10 which is confirm maximum uptake of diprotic dye EBT takes place at pH 3 and 10. However, the adsorption capacity for EBT decreased with increasing pH values to 7. But, when pH was increased from to 10, the adsorption capacity significantly increased. The optimum pH for the adsorbents could be said to be pH 10. At higher pH (basic medium) can be attributed to the increase in negative charged hydroxide ions. In contrast, at lower pH (acidic medium) can be attributed to the increase in positively charged ions. The negative charged hydroxide ions and positively charged ions in solution leads to development of either positive or negative charge on the surface (Şahin et al., 2013). In an alkaline medium, generally two phenomena occur; generation of the most active sites on the catalyst surface and also increasing hydroxyl radical concentrations. It was observed that the concentration of hydroxyl groups can be enhanced by increasing pH. Accordingly, the formation of the hydroxyl radicals increased in the solution and dye degradation achieved superior value. The $H_2O_2$ and $HO_2$ radicals were formed due to the reaction of $\cdot OH - \cdot OH$ radicals. Due to the presence of high amounts of $\cdot OH$ radicals, the radical-radical reactions takes place at higher pH values (Kazeminezhad and Sadollahkhani, 2014; Ejhieh and Khorsandi, 2010). Hence, it can be

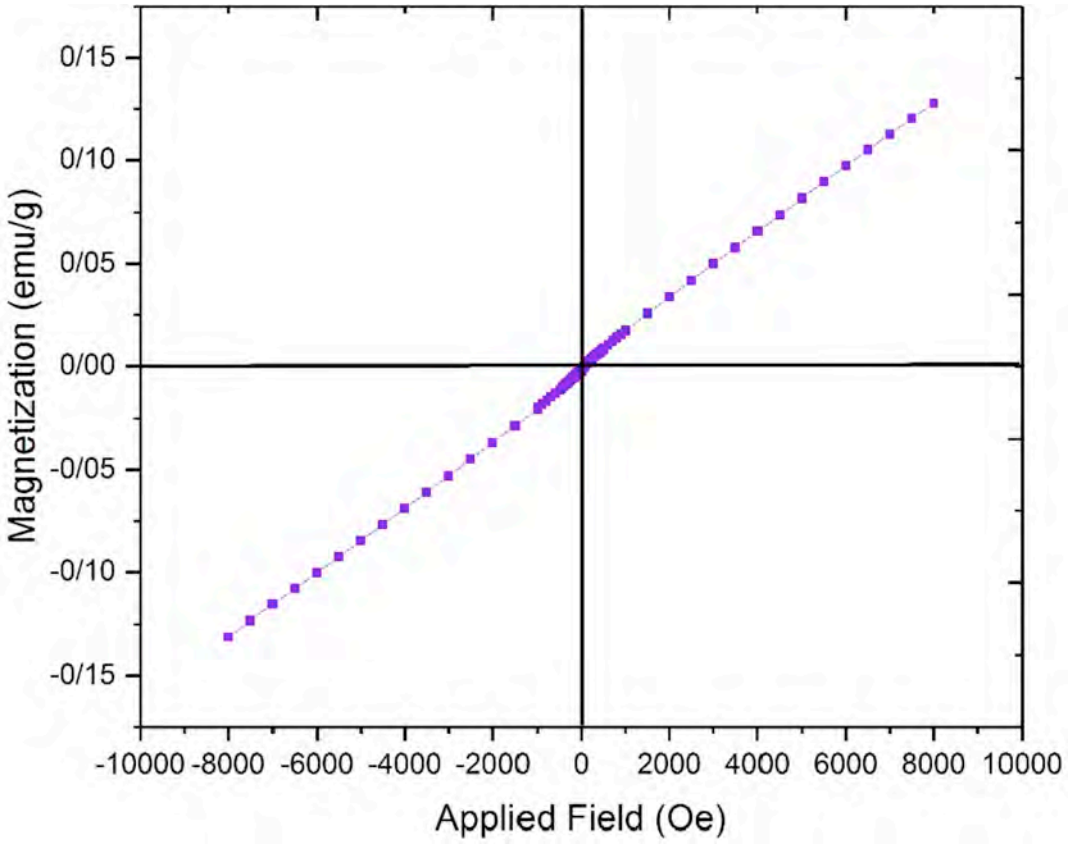


**Fig. 7.** Magnetization versus utilized magnetic field at room temperature for $NdVO_4$ nanoparticles (Sample No. 7).

concluded that there is a direct relation between the pH and decolorization efficiency.

### 3.3.4. *Effect of light source*

Under visible light, 46.74% EBT is removed by $NdVO_4$ nanoparticles after 120 min. In contrast, UV irradiation can remove 72.98% EBT after 75 min (Fig. 10b). Also, a blank test was conducted without any catalyst to investigate degradation of dye under UV irradiation. The results clearly indicate that the degradation of EBT under UV light is negligible (~8%).

### 3.3.5. *Studying of recyclability and stability of catalyst*

To test the repeatability of the $NdVO_4$ nano-photocatalysts, a recycling test of the photodegradation of EBT was performed. Typically, after the first run under UV irradiation, the photocatalysts was separated and washed with distilled water and acetone. Fresh dye solution was mixed up with above used nanocatalysts to start the second run photocatalytic test. After the first run, the subsequent 4 runs of photocatalytic recycling tests were conducted in a similar way. As shown in Fig. 11a, after 6 times recycling photoactivity test, the adsorption capacities depressed slightly from 72.98% to 63.97%. The photocatalytic test for optimum condition repeated and each data point and error bar represents the mean and the standard errors, respectively, of independent triplicates (Fig. 11b). Average percentage degradation of 5 ppm EBT at pH = 11 under UV irradiation with standard deviations are listed in Table 3.

In order to investigate the stability of $NdVO_4$ nano-photocatalysts, fresh sample was prepared and used (Fig. 12). On the basis of its XRD pattern (Fig. 12a), there is no any significant alteration in the characteristic diffraction peaks of $NdVO_4$ nanocatalysts after photocataliyc test after 6 times recycling. The FT-IR spectrum of $NdVO_4$ nanocatalysts after photocatalytic test remains almost unchanged (Fig. 12b). However, a partial alteration after 6 run recycling test can be observed, most probably due to the remaining EBT dye on the surface of the nanoparticles. Stretching vibration bands of the azo group (-N=N-) and $-NO_2$ appears at 1505 $cm^{-1}$ and 1390 $cm^{-1}$, respectively (Bartošová et al., 2017). The results confirm the excellent photostability of as-synthesized $NdVO_4$ nanocatalysts under UV light after 6 cycles. Part of the dye removal process can be associated with dye adsorption. In order to analyze this occurrence, FT-IR of catalyst after photocatalyst test was studied. The FT-IR of $NdVO_4$ after photocatalytic process shows the partial adsorption of EBT dye on the surface of the nanoparticles, but the highest percentage of degradation was affected by photocatalytic properties of as made $NdVO_4$ catalyst. The photocatalytic mechanism of $NdVO_4$ can be proposed on the basis of molecular excitation processes which is investigated in section 3.3.6.

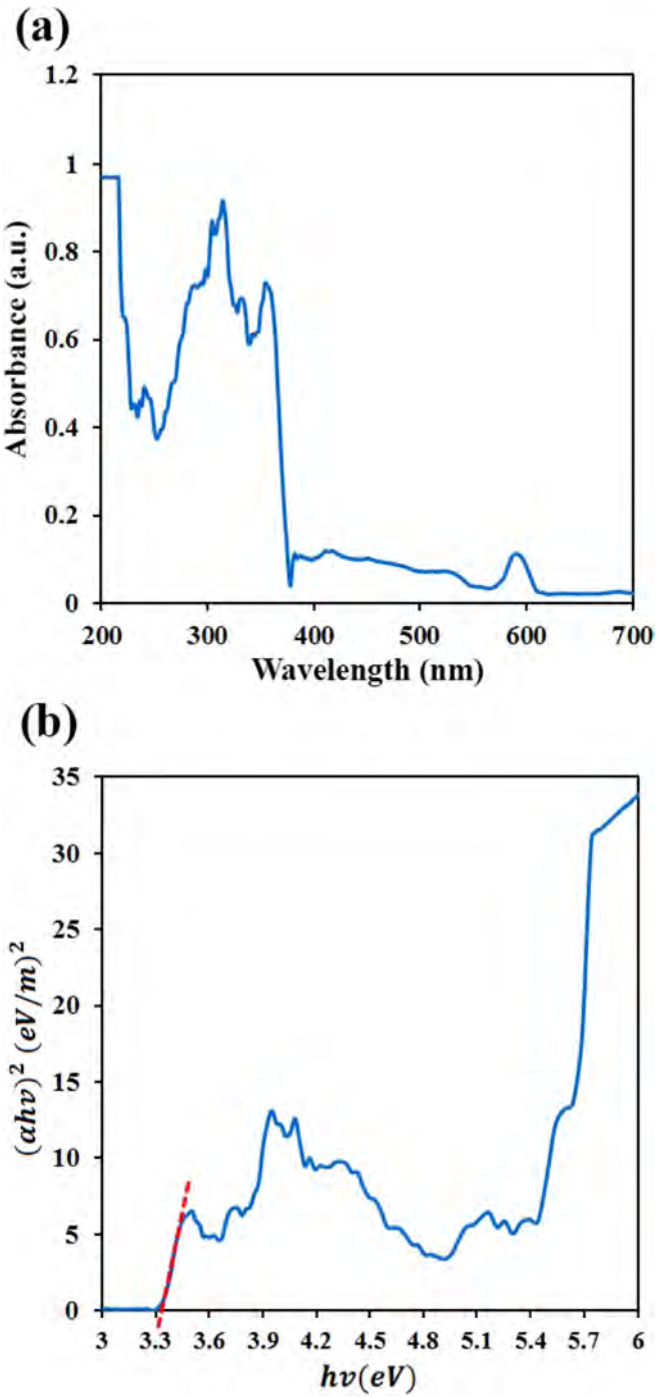


**Fig. 8.** (a) UV–vis spectra and b) plot of (αhν) 2 versus (hν) of $NdVO_4$ nanoparticles (Sample No. 7).

*3.3.6. Studying photodegradation mechanism of catalyst*

To study the photodegradation of dye, plausible mechanisms can be proposed on the basis of molecular excitation processes. As $NdVO_4$ nanoparticles excited by light irradiation, the electron and hole can be formed, where can further react with oxygen and water in environment and produce a series of active sites such as OH and $O_2$ radials (Eq. (2)–(4)). The hole can oxidize water to hydroxyl radicals and the electron can combin with an oxygen molecule to create superoxide radicals (Lee et al., 2015). According to Eq. (5)–(8) these radicals play an important role in the destruction of pollutants.

$$NdVO_4 + h\nu \rightarrow NdVO_4(e^-_{CB} + h^+_{VB}) \quad (2)$$

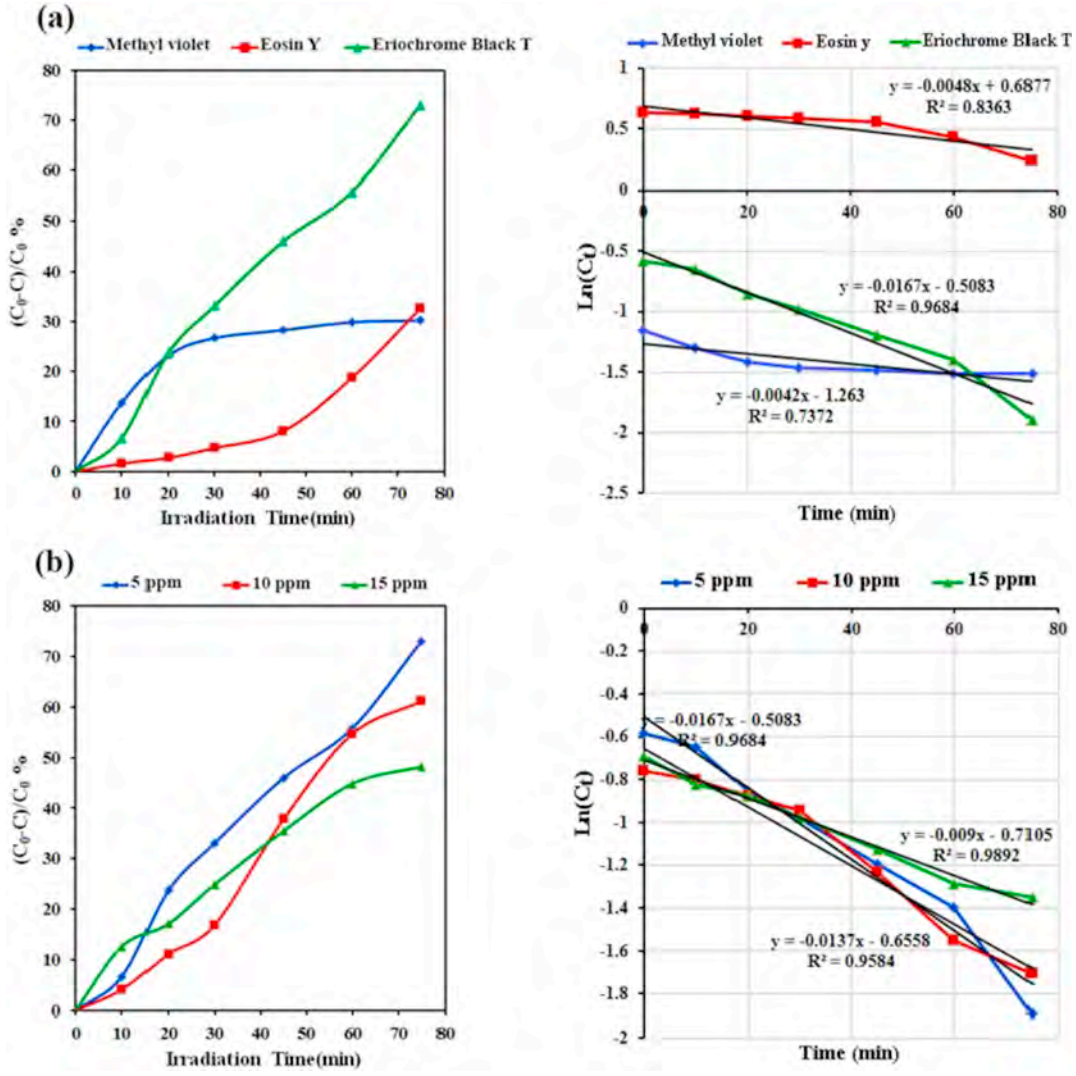


**Fig. 9.** Photocatalytic degradation of Sample No. 7 and plot of ln $C_t$ versus reaction time (a) influence of type of dye and (b) influence of dye concentration.

$$H_2O + h^+_{VB} \longrightarrow \bullet OH + H^+ \quad (3)$$

$$O_2 + e^-_{CB} \longrightarrow O_2^{-\bullet} \quad (4)$$

$$O_2^{-\bullet} + e^-_{CB} + 2H^+ \longrightarrow H_2O_2 \quad (5)$$

$$2O_2^{-\bullet} + 2H^+ \longrightarrow O_2 + H_2O_2 \quad (6)$$

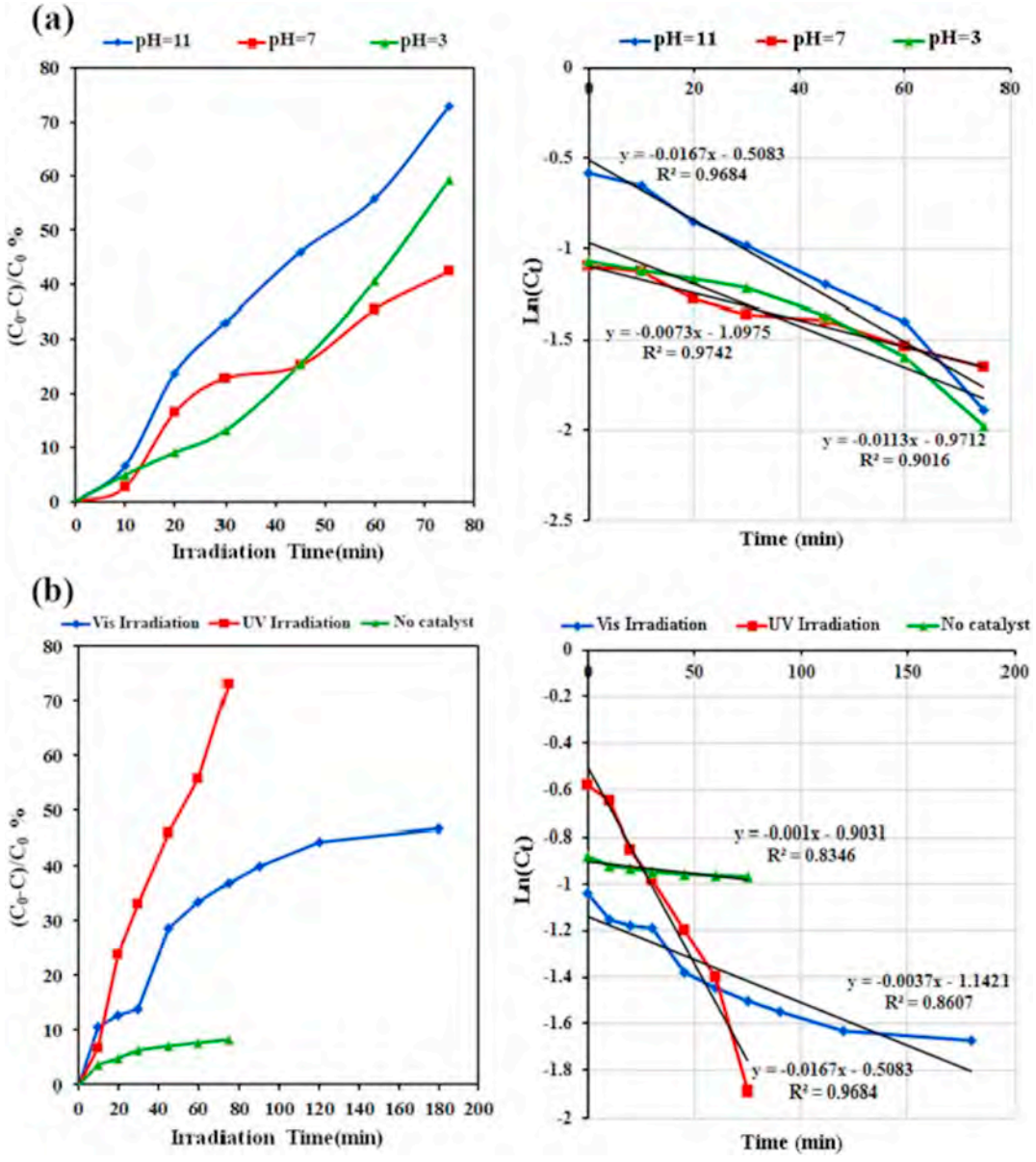


**Fig. 10.** Photocatalytic degradation of Sample No. 7 and plot of ln $C_t$ versus reaction time a) influence of pH and b) influence of light source.

$$H_2O_2 + e^-_{CB} \longrightarrow OH^- + \bullet OH \quad (7)$$

$$Dye + (O_2^{-\bullet} \text{ or } \bullet OH) \longrightarrow intermediate \longrightarrow pruduct + CO_2 + H_2O \quad (8)$$

*3.3.7. Kinetic studies*

The photocatalytic degradation kinetic of many organic dyes have often modeled with Langmuir-. Hinshelwood mechanism (Kazeminezhad and Sadollahkhani, 2014):

$$r = -dC/dt = (kKC)/(1 + KC) \quad (9)$$

where r is the degradation rate of the reactant (mg/L min), C is the concentration of the reactant (mg/L), t is the irradiation time, k is the reaction rate constant (mg/L min), K is the adsorption constant of the reactant (L/mg). When C is very small, the equation can be simplified to:

$$\ln(C_0/C_t) = kKt = K_{app}t \quad (10)$$

$$\ln(Ct) = \ln(C_0) - K_{app}t \quad (11)$$

where $K_{app}$ is the apparent first-order rate constant given by the slope of

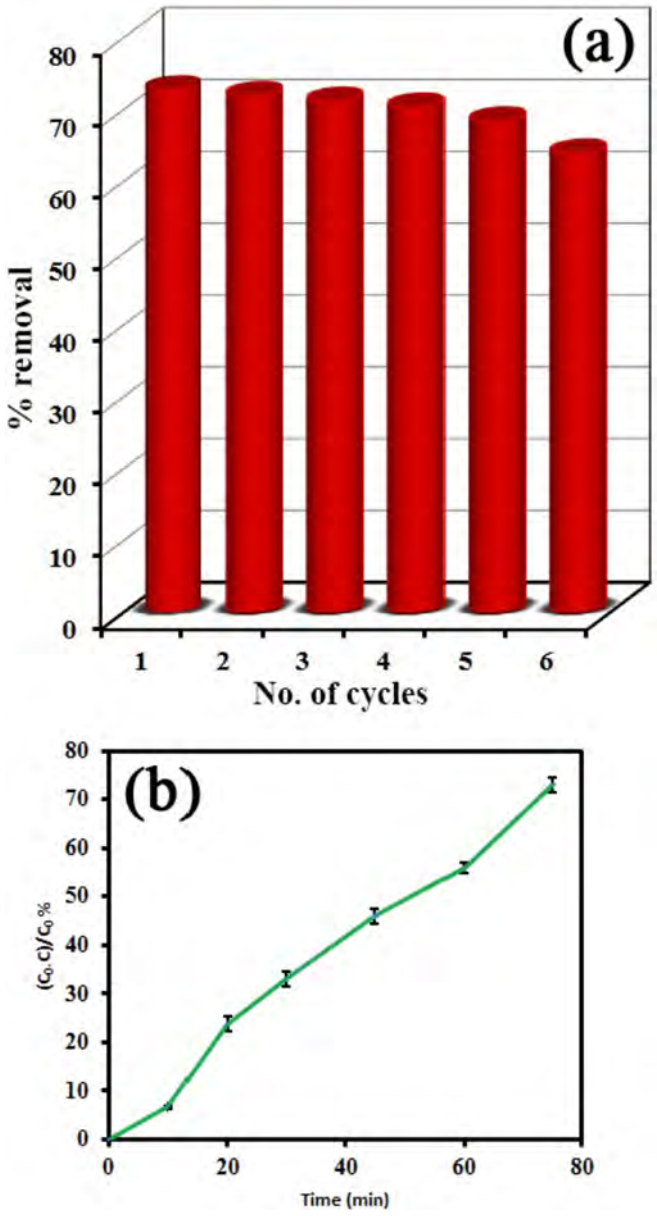


**Fig. 11.** (a) Recycling experiments for sample No. 7 after 6 cycles photocatalytic activity (b) presentation of error bar after repeat photocatalytic test sampling for sample No. 7 (Each data point and error bar represents the mean and the standard errors, respectively, of independent triplicates, Error bar = ± 1S.D.).

**Table 2**
Crystallite and particle sizes of as-synthesized product obtained from XRD and SEM results.

| Sample No. | Average crystallite diameter (nm) | Average particle size (nm) |
|---|---|---|
| 1 | – | 513.58 |
| 2 | – | 493.10 |
| 3 | 33.62 | 283.42 |
| 4 | 37.58 | 457.97 |
| 5 | 32.89 | 104.04 |
| 6 | 34.50 | 304.06 |
| 7 | 30.25 | 79.98 |
| 8 | 32.20 | – |
| 9 | 24.54 | – |

the graph of $\ln(C_o/C_t)$ vs. t and $C_o$ is the initial concentration of the reactant. If Eq. (11) is compared with the equation of straight line $y = mx + c$, a plot of $\ln C_t$ versus t should give a straight line whose slope is $-k_{app}$. The intercept of the plot is $\ln C_0$. the plots of Ln ($C_t$) versus time for all samples are clearly seen in Figs. 9 and 10 the results are in agreement with the first order kinetic behavior. In Table 3 were given the correlation coefficient ($R^2$) values. These values confirm that the photocatalytic reactions in this work followed the Pseudo-first order kinetic (Mahdiani et al., 2018). If a substance A is undergoing transformation such that its apparent concentration remains constant during the process, the following expression holds true.

## 4. Conclusion

The aim of this project was to assess favorable nano-photocatalysts with uniform and small size. For this reason, $H_2$acacen was used as a capping agent to prevent agglomeration of products in the solid state process. Several parameters were compared to reach optimum size and uniformity of as-made samples. These factors include calcination time, calcination temperature, and molar ratio of $H_2$acacen. The best size of particle is achieved when ratio of $H_2$acacen to Nd was 2:1 and calcined at 700 °C for 2 h. The influence of different parameters such as type of dye, type of light source, pH and dye concentration on photocatalytic activity of samples were investigated. So, the prepared catalyst shows 77.98% photocatalytic efficiency in degradation of 5 ppm Eriochorome Black T under UV light at pH = 11 which can be promising material to improve the catalytic performance for contaminant. Our findings suggest that the $NdVO_4$ nanoparticles is a potential nano-photocatalysts for dye removal from waste water. Thus, our belief is that the nanosized $NdVO_4$ nanoparticles can be used as a promising photocatalysts in various industries.

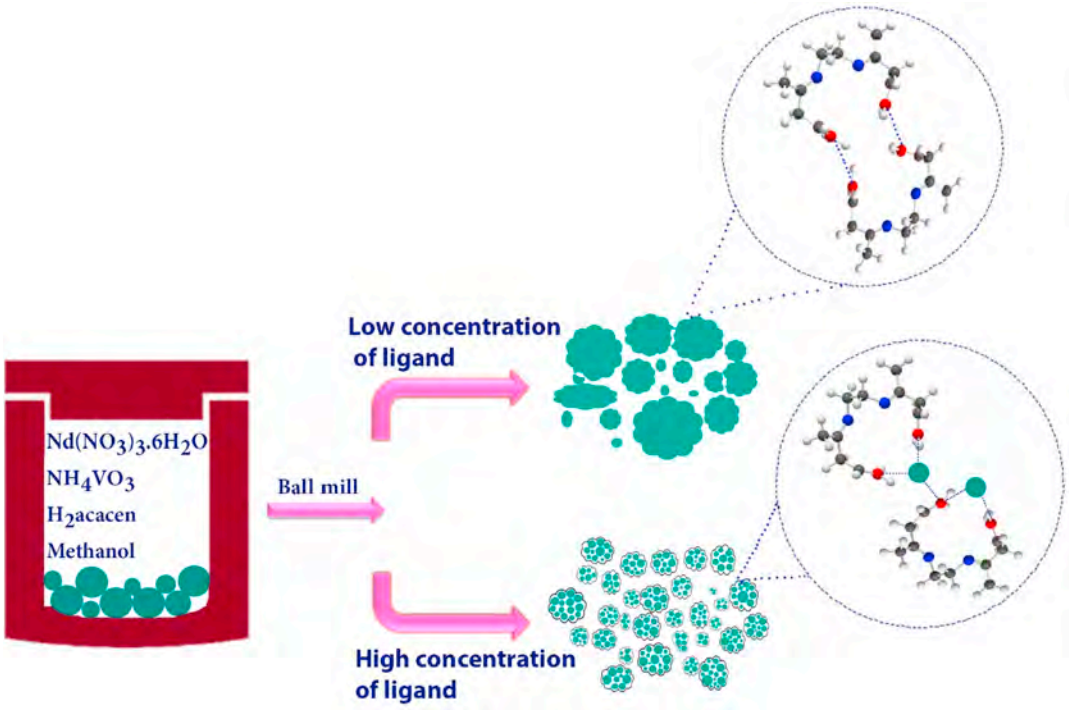


**Scheme 1.** Schematic illustration for the preparation of $NdVO_4$ nanostructures.

**Table 3**
Average percentage degradation of 5 ppm EBT at pH = 11 under UV irradiation with standard deviations.

| Time (min) | 1st Run | 2nd Run | 3rd Run | Ave. | S.D. |
|---|---|---|---|---|---|
| 0 | 0 | 0 | 0 | 0 | 0 |
| 10 | 6/618962 | 6/870229 | 7/495069 | 6/994753 | 0/451132 |
| 20 | 23/79249 | 21/18321 | 21/30178 | 22/09249 | 1/473434 |
| 30 | 33/09481 | 34/92366 | 36/09467 | 34/70438 | 1/511905 |
| 45 | 45/97496 | 44/08397 | 46/9428 | 45/66724 | 1/454044 |
| 60 | 55/81395 | 54/38931 | 56/41026 | 55/53784 | 1/038379 |
| 75 | 72/98748 | 70/80153 | 73/57002 | 72/45301 | 1/459583 |

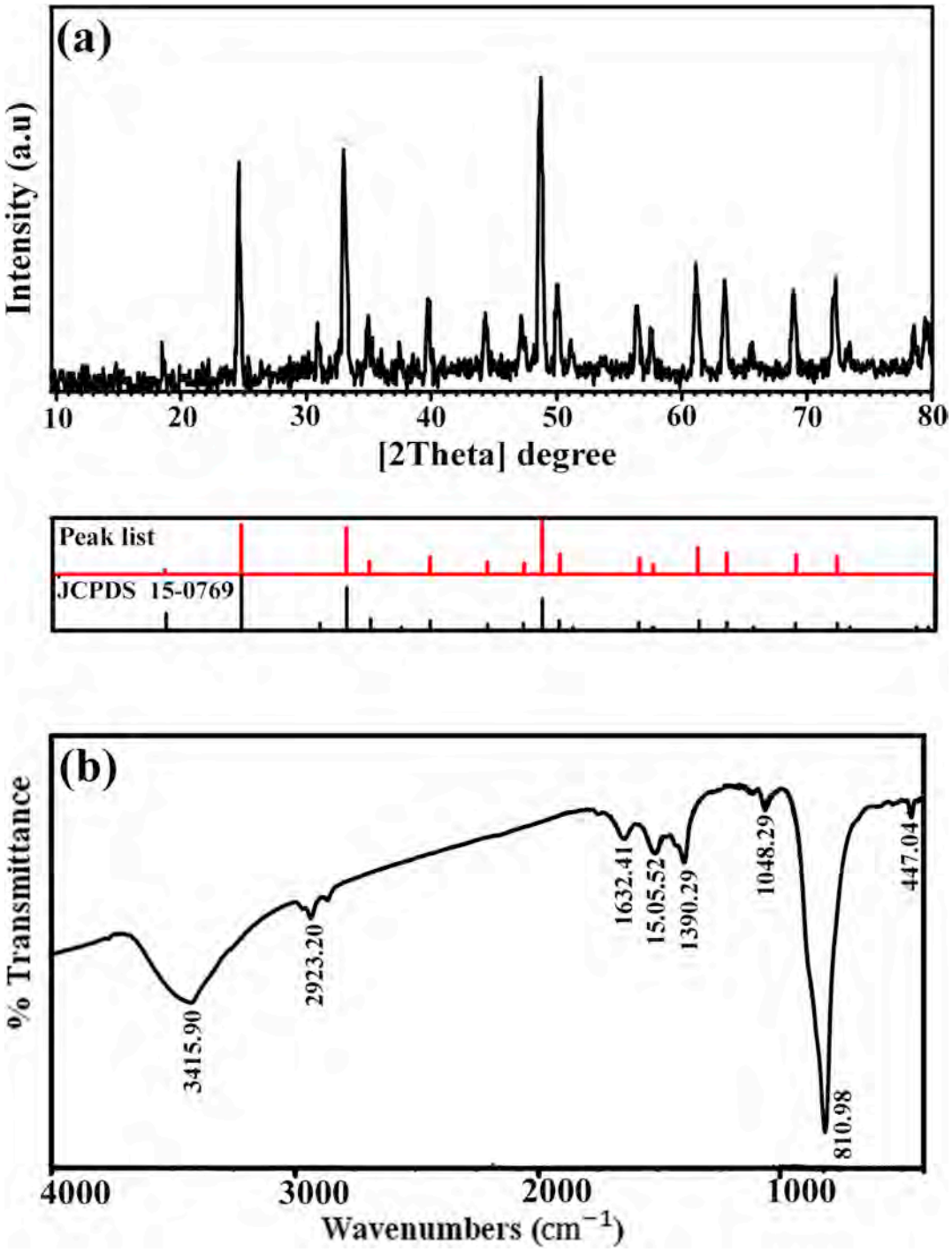


**Fig. 12.** (a) XRD pattern and (b) FT-IR spectrum of $NdVO_4$ nano-photocatalyst after photocatalytic activity.

## Acknowledgements

Authors are grateful to the council of Iran National Science Foundation (INSF) and University of Kashan for supporting this work by Grant No (159271/1892290).

## References

Au, C., Zhang, W., Wan, H., 1996. Preparation and characterization of rare earth orthovanadates for propane oxidative dehydrogenation. Catal. Lett. 37, 241–246.

Bartošová, A., Blinová, L., Sirotiak, M., Michalíková, A., 2017. Usage of FTIR-ATR as non-destructive analysis of selected toxic dyes. Res. Pap. Faculty Mater. Sc. Technol. Slovak Univ. Technol. 25, 103–111.

de Luna, M.D.G., Flores, E.D., Genuino, D.A.D., Futalan, C.M., Wan, M.-W., 2013. Adsorption of Eriochrome Black T (EBT) dye using activated carbon prepared from waste rice hulls—optimization, isotherm and kinetic studies. J. Taiwan Inst. Chem. Eng. 44, 646–653.

Deng, H., Yang, S., Xiao, S., Gong, H.-M., Wang, Q.-Q., 2008. Controlled synthesis and upconverted avalanche luminescence of cerium (III) and neodymium (III) orthovanadate nanocrystals with high uniformity of size and shape. J. Am. Chem. Soc. 130, 2032–2040.

Dragomir, M., Arčon, I., Gardonio, S., Valant, M., 2013. Phase relations and optoelectronic characteristics in the $NdVO_4$–$BiVO_4$ system. Acta Mater. 61 (4), 1126–1135.

Ejhieh, A.N., Khorsandi, M., 2010. Photodecolorization of Eriochrome Black T using NiS–P zeolite as a heterogeneous catalyst. J. Hazard Mater. 176, 629–637.

Elijah, O.C., Nwabanne, J., 2014. Adsorption studies on the removal of Eriochrome black-T from aqueous solution using Nteje clay. SOP Trans. Appl. Chem. 1, 14–25.

Errandonea, D., Popescu, C., Achary, S., Tyagi, A., Bettinelli, M., 2014. In situ high-pressure synchrotron X-ray diffraction study of the structural stability in $NdVO_4$ and

$LaVO_4$. Mater. Res. Bull. 50, 279–284.
Ghiyasiyan-Arani, M., Masjedi-Arani, M., 2016. Size controllable synthesis of cobalt vanadate nanostructures with enhanced photocatalytic activity for the degradation of organic dyes. J. Mol. Catal. A: Chem. 425, 31–42.
Ghiyasiyan-Arani, M., Masjedi-Arani, M., Salavati-Niasari, M., 2016a. Novel Schiff base ligand-assisted in-situ synthesis of Cu $_3$ V $_2$ O $_8$ nanoparticles via a simple precipitation approach. J. Mol. Liq. 216, 59–66.
Ghiyasiyan-Arani, M., Masjedi-Arani, M., Ghanbari, D., Bagheri, S., Salavati-Niasari, M., 2016b. Novel chemical synthesis and characterization of copper pyrovanadate nanoparticles and its influence on the flame retardancy of polymeric nanocomposites. Sci. Rep. 6.
Ghiyasiyan-Arani, M., Masjedi-Arani, M., Salavati-Niasari, M., 2016c. Facile synthesis, characterization and optical properties of copper vanadate nanostructures for enhanced photocatalytic activity. J. Mater. Sci. Mater. Electron. 27, 4871–4878.
Ghiyasiyan-Arani, M., Salavati-Niasari, M., Naseh, S., 2017. Enhanced photodegradation of dye in waste water using iron vanadate nanocomposite; ultrasound-assisted preparation and characterization. Ultrason. Sonochem. 39, 494–503.
Ghiyasiyan-Arani, M., Salavati-Niasari, M., Masjedi-Arani, M., Mazloom, F., 2018. An easy sonochemical route for synthesis, characterization and photocatalytic performance of nanosized FeVO4 in the presence of aminoacids as green capping agents. J. Mater. Sci. Mater. Electron. 29, 474–485.
Jing, X., Chenguo, H., Gaobin, L., Hong, L., Guojun, D., Yan, Z., 2011. Synthesis and visible-light photocatalytic activity of NdVO4 nanowires. J. Alloys Compounds 509, 7968–7972.
Kazeminezhad, I., Sadollahkhani, A., 2014. Photocatalytic degradation of Eriochrome black-T dye using ZnO nanoparticles. Mater. Lett. 120, 267–270.
Klung, H., Alexander, L., 1962. X-ray Diffraction Procedures, vol. 491 Willey, New York, EUA.
Lee, K.M., Hamid, S.B.A., Lai, C.W., 2015. Multivariate analysis of photocatalytic-mineralization of Eriochrome Black T dye using ZnO catalyst and UV irradiation. Mater. Sci. Semicond. Process. 39, 40–48.
Lyadov, A.S., Kurilkin, V.V., 2016. Reduction specifics of rare-earth orthovanadates (REE = La, Nd, Sm, Dy, Ho, Er, Tm, Yb, and Lu). Russ. J. Inorg. Chem. 61, 86–92.
Mahapatra, S., Madras, G., Guru Row, T., 2007. Synthesis, characterization and photocatalytic activity of lanthanide (Ce, Pr and Nd) orthovanadates. Ind. Eng. Chem. Res. 46, 1013–1017.
Mahapatra, S., Nayak, S.K., Madras, G., Guru Row, T., 2008a. Microwave synthesis and photocatalytic activity of nano lanthanide (Ce, Pr, and Nd) orthovanadates. Ind. Eng. Chem. Res. 47, 6509–6516.
Mahapatra, S., Vinu, R., Row, T.G., Madras, G., 2008b. Kinetics of photoconversion of cyclohexane and benzene by LnVO 4 and LnMo 0.15 V 0.85 O 4 (Ln = Ce, Pr and Nd). Appl. Catal. Gen. 351, 45–53.
Mahdiani, M., Soofivand, F., Ansari, F., Salavati-Niasari, M., 2018. Grafting of $CuFe_{12}O_{19}$ nanoparticles on CNT and graphene: eco-friendly synthesis, characterization and photocatalytic activity. J. Clean. Prod. 176, 1185–1197.
Mazloom, F., Masjedi-Arani, M., Ghiyasiyan-Arani, M., Salavati-Niasari, M., 2016. Novel sodium dodecyl sulfate-assisted synthesis of Zn $_3$ V $_2$ O $_8$ nanostructures via a simple route. J. Mol. Liq. 214, 46–53.
Mendhulkar Vijay, D., Anu, Y., Supriya, K., Photochemical Decolorization of Methyl Violet Dye Using Azadirachta indica (Neem) Mediated Synthesized Silver Nanoparticles.
Monsef, R., Ghiyasiyan-Arani, M., Salavati-Niasari, M., 2018. Application of ultrasound-aided method for the synthesis of $NdVO_4$ nano-photocatalyst and investigation of eliminate dye in contaminant water. Ultrason. Sonochem. 42, 201–211.
Motahari, F., Mozdianfard, M.R., Salavati-Niasari, M., 2015. Synthesis and adsorption studies of NiO nanoparticles in the presence of H 2 acacen ligand, for removing Rhodamine B in wastewater treatment. Process Saf. Environ. Protect. 93, 282–292.
Nguyen, A.-D., Murdoch, K., Edelstein, N., Boatner, L., Abraham, M., 1997. Polarization dependence of phonon and electronic Raman intensities in PrVO $_4$ and NdVO $_4$. Phys. Rev. B 56, 7974.
Oyelude, E.O., Awudza, J.A., Twumasi, S.K., 2017. Equilibrium, kinetic and thermodynamic study of removal of Eosin yellow from aqueous solution using teak leaf litter powder. Sci. Rep. 7, 12198.
Şahin, Ömer, Saka, Cafer, Kutluay, Sinan, 2013. Cold plasma and microwave radiation applications on almond shell surface and its effects on the adsorption of Eriochrome Black T. J. Ind. Eng. Chem. 19, 1617–1623.
Selvan, R.K., Gedanken, A., Anilkumar, P., Manikandan, G., Karunakaran, C., 2009. Synthesis and characterization of rare earth orthovanadate (RVO 4; Rá = áLa, Ce, Nd, Sm, Eu & Gd) nanorods/nanocrystals/nanospindles by a facile sonochemical method and their catalytic properties. J. Cluster Sci. 20, 291–305.
Vaiano, V., Matarangolo, M., Sacco, O., Sannino, D., 2017. Photocatalytic treatment of aqueous solutions at high dye concentration using praseodymium-doped ZnO catalysts. Appl. Catal. B Environ. 209, 621–630.
Verma, S., Gupta, R., Bamzai, K., 2016. Effect of mixing $Ce^{3+}$ and $Nd^{3+}$ ions in equimolar ratio on structural, optical and dielectric properties on pure cerium orthovanadate and neodymium orthovanadate. Mater. Res. Bull. 81, 71–84.
Vosoughifar, M., 2016. Synthesis, characterization, and investigation magnetic and photocatalytic property of neodymium vanadate nanoparticles. J. Mater. Sci. Mater. Electron. 27, 7384–7388.
Wu, X., Tao, Y., Dong, L., Zhu, J., Hu, Z., 2005. Preparation of single-crystalline $NdVO_4$ nanorods, and their emissions in the ultraviolet and blue under ultraviolet excitation. J. Phys. Chem. B 109, 11544–11547.
Yao, B., Wu, K., Zhang, C., Zhang, H., Wang, Z., Wang, J., Yu, H., Yu, Y., Jiang, M., 2010. Crystal growth and laser performance of neodymium-doped scandium orthovanadate. J. Cryst. Growth 312, 720–723.
Yuvaraj, S., Selvan, R.K., Kumar, V.B., Perelshtein, I., Gedanken, A., Isakkimuthu, S., Arumugam, S., 2014. Sonochemical synthesis, structural, magnetic and grain size dependent electrical properties of $NdVO_4$ nanoparticles. Ultrason. Sonochem. 21, 599–605.